REPORT DOCUMENTATION PAGE

Form Approved OMB No. 0704-0188

1. REPORT DATE *(DD-MM-YYYY)* 04-11-2008	2. REPORT TYPE: final	3. DATES COVERED *(From - To)* 03/15/ 2005 to 10/15/2008

4. TITLE AND SUBTITLE
Agile Response Coatings

5a. CONTRACT NUMBER

5b. GRANT NUMBER FA9550-05-1-0234

5c. PROGRAM ELEMENT NUMBER

6. AUTHOR(S) David L. Carroll

5d. PROJECT NUMBER

5e. TASK NUMBER

5f. WORK UNIT NUMBER

7. PERFORMING ORGANIZATION NAME(S) AND ADDRESS(ES)

Wake Forest University
Department of Physics
Winston-Salem NC 27109

8. PERFORMING ORGANIZATION REPORT NUMBER

9. SPONSORING / MONITORING AGENCY NAME(S) AND ADDRESS(ES)
AFOSR/NL
4015 Wilson Blvd, Room 713
Arlington, VA 22203-1954
c/o Dr. Charles Y-C Lee

10. SPONSOR/MONITOR'S ACRONYM(S)
AFOSR

11. SPONSOR/MONITOR'S REPORT NUMBE AFRL-OSR-VA-TR-2013-0917

12. DISTRIBUTION / AVAILABILITY STATEMENT

Distribution A: Approved for Public Release

13. SUPPLEMENTARY NOTES

20130918431

14. ABSTRACT

The mission of the Agile Response Coatings (ARC) program is to address areas of critical need through embedding sensing and response capabilities into a coating system compatible with a wide range of air force weapons and surveillance platforms. The program is intended to develop a coating system that biomemetically responds to its surroundings, airframe integrity, and attack. To do this, the program will design and engineer a set of sensing technologies and camouflage technologies based on novel nano-structured composite materials. We ultimately envisage these to be integrated into a distributed system of autonomous response.

15. SUBJECT TERMS

16. SECURITY CLASSIFICATION OF:			17. LIMITATION OF ABSTRACT	18. NUMBER OF PAGES	19a. NAME OF RESPONSIBLE PERSON
a. REPORT	b. ABSTRACT	c. THIS PAGE		19	David Carroll
					19b. TELEPHONE NUMBER *(include area code)* 336 758 5508

SUMMARY STATEMENT

Through the use of electroactive nanocomposite technology this program has demonstrated a wide range of technologies as described in our deliverables above. Specifically,

1) Enhanced electrochromic response using metal-nanoparticle enhancement through coupling to Plasmon modes in an EAP electrochromic host has been demonstrated.
2) Gas sensor technology with "gain" due to Fermi level pinning of the nanoparticulate phase has provided the first demonstration of a potentially new sensing scheme.
3) Pressure sensing technology, with robust application profiles, have been developed.
4) Synthesis of new "multigap polymers" for broad band sensing is currently underway.

4.0 PROGRAM RESULTS

Enhanced electrochromic response

When the regular order is removed in the system above, the overall optics is dominated by turbid scatter as would be expected. However, when the individual nanoparticles of the meso-phase have a well defined oscillator strengths (as in the case of plasmonic particles), both near and far field interactions within that nanocomposite dispersion can be observed. This is the case when looking at electrochromism in the host. In this case both charge exchange to the particle from the excitations, and meso-scale dielectric interactions come into play. Specifically, we have shown that the meso-scale dispersion of particles modifies the local dielectric, yielding a shift in the plasmonic bands of the nanophase, and the mobility of excitons are also shifted due to local trapping effects.

Description

To make this demonstration, electrochromic devices were made using a nanocomposite blend of conducting polymer poly(3,4 ethylenedioxythiophene): poly styrene sulfonate (PEDOT:PSS) and metal nanoparticles of silver or gold. Microscopic analysis showed a random distribution of metal nanoparticles with little aggregation in the matrix. The two terminal devices exhibited an increase in absorption that is dependant on the loading of nanoparticles in the polymer. Further, the active electrochromic spectral window showed a bias dependant tuning and a broadened spectral response. All devices exhibited slow relaxivities which we interpret as resulting from the high capacitance of the metal nanoparticles embedded in the polymer matrix.

Results

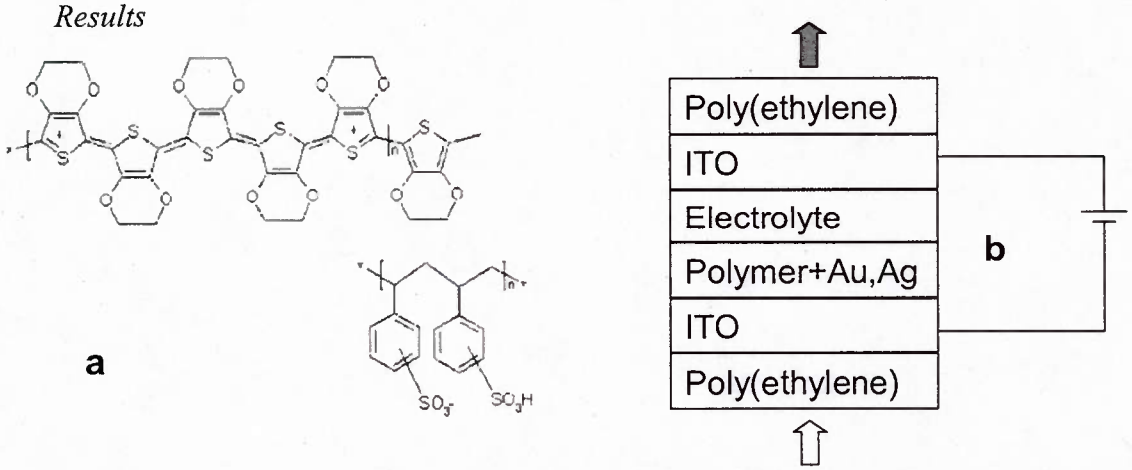

Figure 4.1. a) Chemical structure of PEDOT: PSS, b). The schematic of the electrochromic device structure

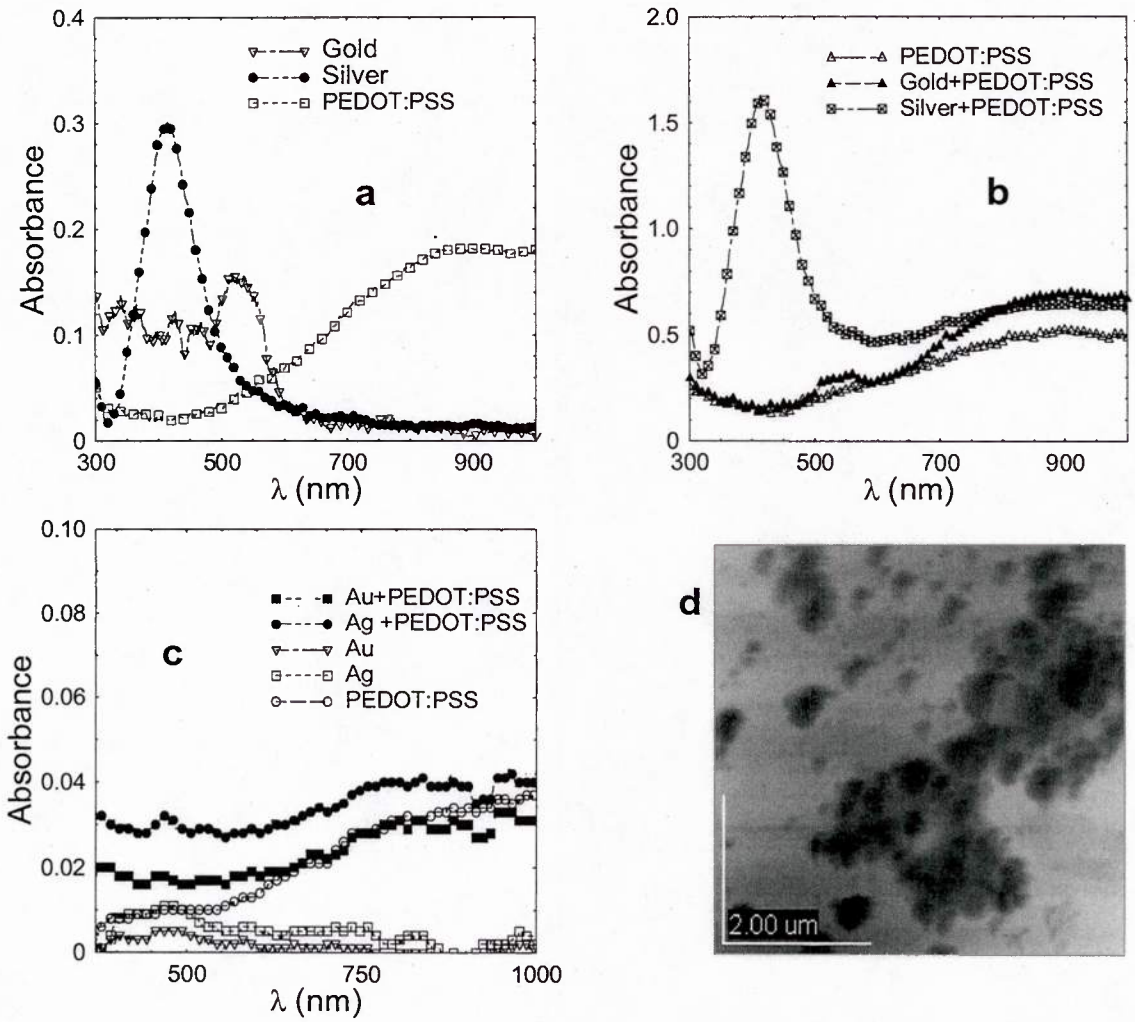

Figure 4.2. a). The absorbance spectrum of dispersion of gold, silver nanoparticles and PEDOT:PSS in water. B) The absorbance spectra of composites mixed in 1:1 ratio of metal nanoparticles dispersion and PEDOT:PSS dispersion. C). The comparison of absorbance spectra of individual thin films and composites thin films. D). AFM (noncontact mode) image of the Au thin film o

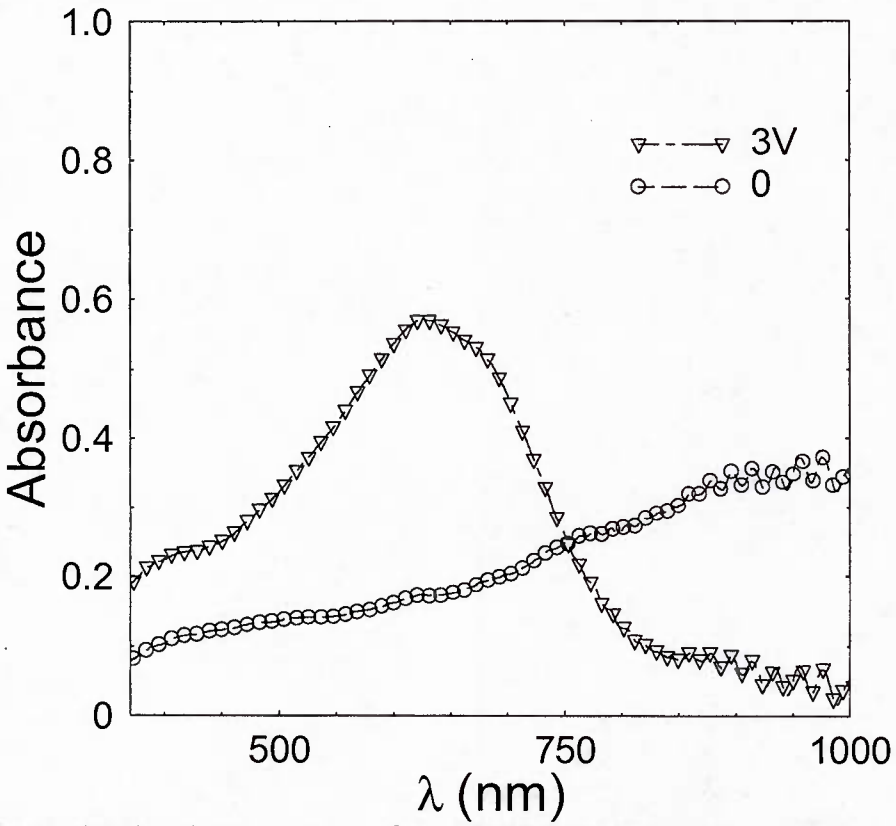

Figure 4.3, The absorbance spectra of the PEDOT: PSS only electrochromic device in different bias conditions

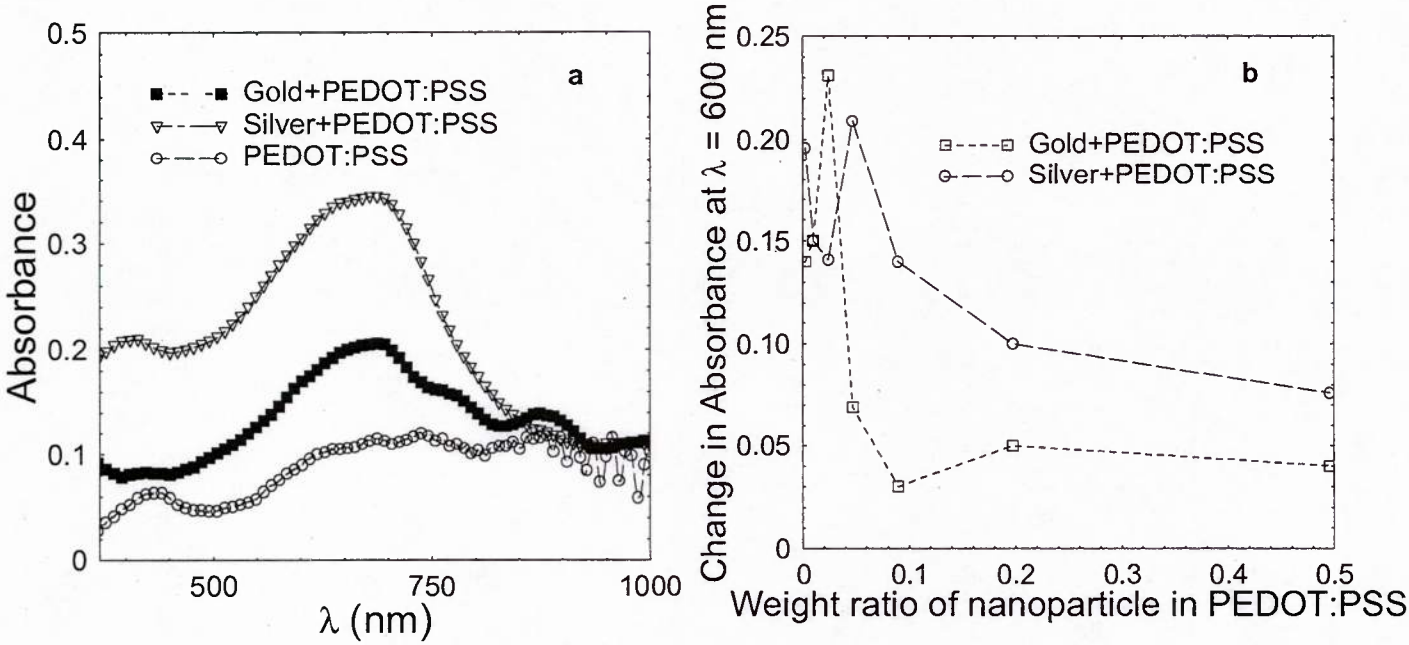

Figure 4.4. a). The electrochromic properties pf the composite b). The absorbance change of the composite device with respect to different loading ratio of the nanoparticles in PEDOT: PSS

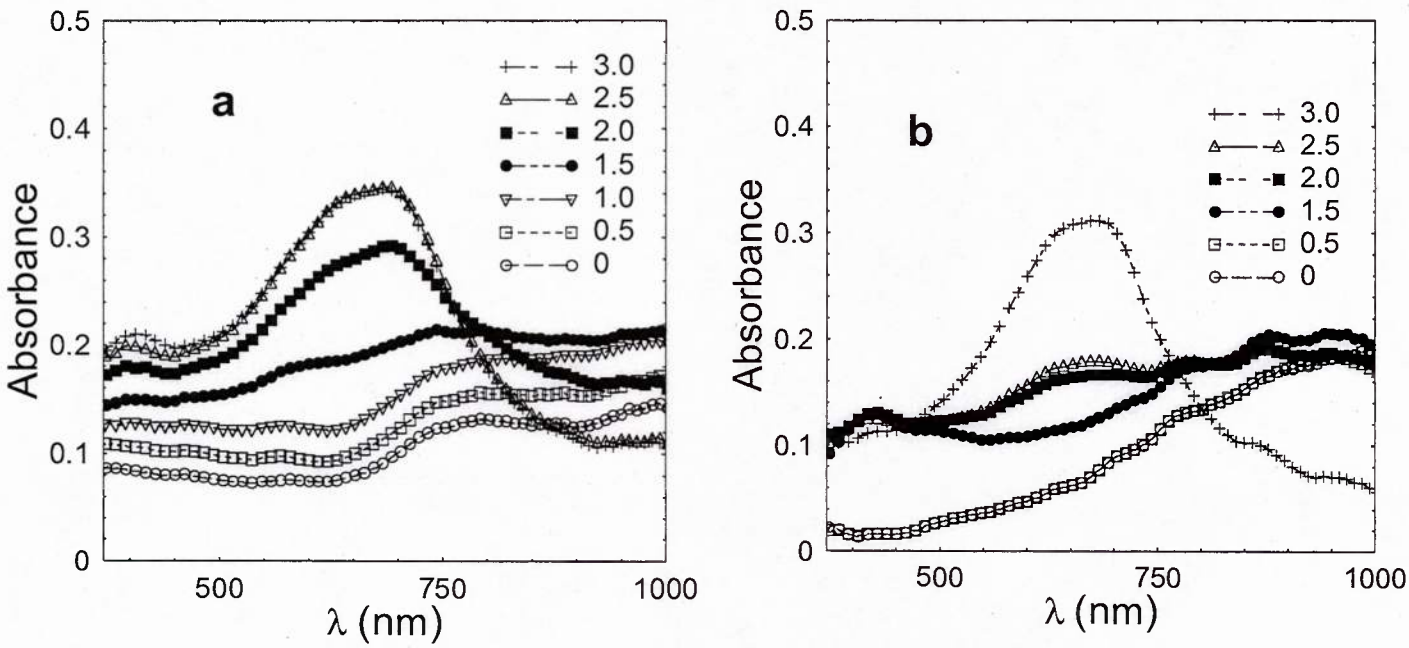

Figure 4.5. a) The bias dependant electrochromic properties of Ag+ PEDOT:PSS composite and b) that of Au+ PEDOT:PSS

This report lists only the major advances of the program and is NOT exhaustive.

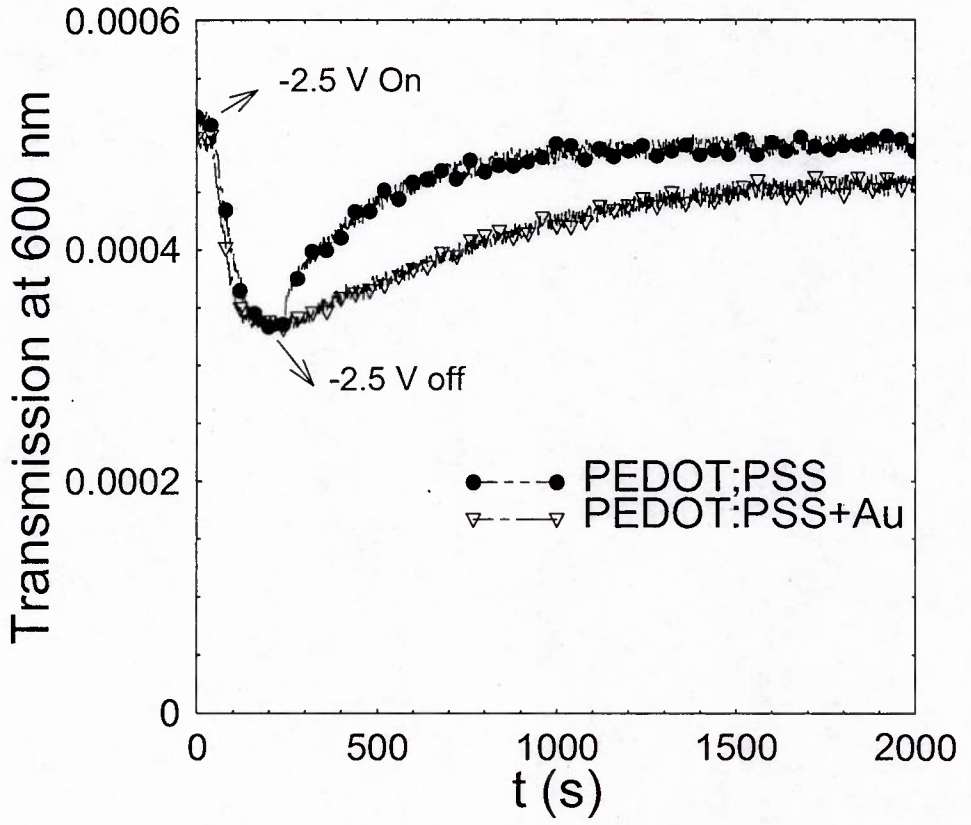

Figure 4.6. The time response of the electrochromc device with respect to voltage ON and OFF state

Summary

Electrochromic devices with nanocomposite blends consisting of metal nanoparticles and conducting polymers were made. The devices showed enhanced absorbance due to luorin absorption in the nanoparticles. The absorbance enhancement depends on the loading of the nanoparticles in PEDOT: PSS as expected. However, the luorin absorption peak depends on the dielectric properties of the surrounding medium allowing tuning of the spectral response with voltage. The color tuning and time response makes this material a prospective candidate for full color electrochromic displays.

Gas Sensors with Gain(description taken from our paper APPLIED PHYSICS LETTERS 91, 203111 -2007)

Semiconducting single-walled carbon nanotubes _SWCNTs_ offer a number of advantages as gas sensors. In particular, SWCNTs change their electrical properties when in contact with gases at room temperature, thus reducing power consumption. In addition, SWCNTs can detect low gas concentration ppb _parts-per-billion_ and ppm _parts-permillion _, and be reusable. However, besides the cost of high-quality pure SWCNTs, the electrical responses to gases depend on several factors. For instance, the particular configuration of the sensor _e.g., the distance between electrodes, the type of contact metals used, whether a two or three-terminal system is used_ and the structural characteristics of the NTs _as individual NTs _e.g., diameter size_ or bundles _e.g., density, presence of metallic NTs in the percolation network__ can affect the overall electrical response to the gases. In the case of field effect transistors, the metal/NT interface has an important role in the electrical changes The particular gas molecules adsorbed onto the NT/metal interface change the metal work function and thus the NT/ metal resistance. Therefore, the electrical changes of the SWCNT were not created by hole doping along the NT surface.

An interesting approach to avoiding the issues using only SNCNTs or CPs is to combine them into nanocomposites. Work has indicated an increase in the stability, conductivity, and polymer strength by the addition of SWCNTs. Thus, by using various analytes that can change the charge transfer dynamics between the SWCNTs and CPs in the nanocomposite, we anticipate a dramatic change in the sensitivity of these chemical devices. We have investigated combining silicon-on-insulator _SOI_ complementary-metal-oxide-semiconductor _CMOS_ microtechnology with nanotechnology. Figure 4.7 shows a schematic representation of the SOI CMOS design. By combining both micro- and nanotechnology, the gas-sensing device can offer a low power consumption _below 10 mW at 100 °C_ due to the use of membrane technology and higher sensitivity/selectivity by using semiconducting SWCNTs and CPs—both SOI compatible. The design and characterization of the SOI device is described in detail elsewhere.

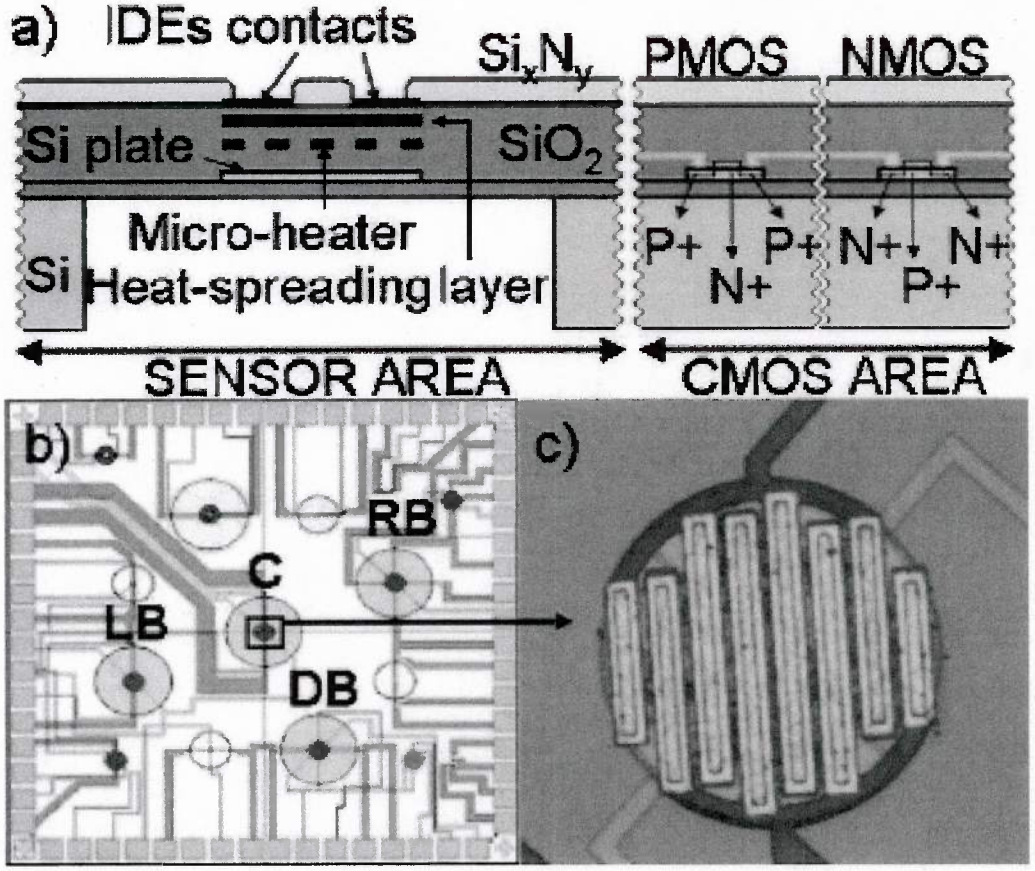

FIG. 1 a Schematic representation of the SOI device with gas sensing area and integrated CMOS circuitry. B Top view representation of the device with four membranes: C, center; RB, right big; LB, left big; DB, down big. C Optical image of the IDEs represented in b with nanocomposite material on top of the electrodes.

The polymer we used was poly(3,3_-dialkyl-quarterthiophone), PQT-12. The main advantages of the polymer are the minimal gate bias stress effect with best thin film transistor (TFT) qualities at ambient fabrication conditions. In addition, it is rather stable in air, moisture, and light, and has high mobility values of 0.08–0.14 cm2/V s.
SWCNTs _HiPco, Carbon Nanotechnologies, Inc., 95%_ and PQT-12 _alkyl chains are 12 carbon atoms long; American Dye Source, Inc._ polymer were dropped directly onto tungsten interdigited electrodes (IDEs) located above the heaters and embedded within the CMOS sequence inside the four membranes _Fig. 1: C, center; LB, left big; DB, down big; RB, right big. The tungsten IDEs 75m diameter have a gap between each arm of approximately 8 m. We used the IDEs instead of the two-contact electrodes to improve the signal-to-noise ratio of the electrical responses and effective electrical contact between NT bundles and metal contacts. To deposit the material efficiently, reducing

costs and resulting in scalability, we chose the ink jet printing Microdrop™ method. The procedure to form the nanocomposite was as follows: the SWCNTs were sonicated in *N*-methylpyrrolidone then deposited by ink-jet printing onto the IDEs, and the solvent was allowed to dry. PQT-12 dissolved in the same solvent was deposited on top of the SWCNTs with the solvent being allowed to dry in ambient conditions. The concentration of NTs used 0.005 mg/mL, and for PQT-12 was 0.05 mg/mL. Figure 1 shows an optical image of the IDEs with a nanocomposite on top. For comparison, one sensor device containing only NTs 0.005 mg/mL and one with only PQT-12 0.05 mg/mL were also prepared. Both the polymer and nanocomposite materials indicated good stability at ambient conditions and under light for the monitored period of 6 months. We labeled the sensor with NTs only as A1, the sensor with pure PQT-12 as A2, and the sensor with the nanocomposite as A3. For gas testing, the three devices containing the sensing material were wire bonded and packaged into a ceramic pin grid array PGA package and placed sequentially onto a printed circuit board socket. The board was placed in a vacuum chamber connected to a rotary (Edwards 18) and turbo pump, with electrical feedthrough and a gas flow inlet and outlet. The pressure inside the vacuum chamber was monitored using an Edwards wide range pressure gauge. The gases tested were nitrogen, hydrogen, ammonia, and acetone. Electrical measurements were performed at room temperature with the wires connected to all the IDEs from the four membranes. The *I-V* characteristics were measured using a Keithley 236 source measurement unit at different partial pressures while allowing the particular analyte in. To test the subsequent gas, the system was pumped down to the original vacuum pressure and kept for 1 h to avoid memory effects from the previous gas tested. We exposed the three sensors to vapor concentrations from 0.01 up to 1000 ppm for 20 s while measuring the changes in electrical behavior. The four gases tested and the four sensing locations utilized resulted in 48 *I-V* plots. To simplify the data, we only show the *I-V* characteristics at different partial pressures from the three devices where the sensing materials were located at the center. Figure 2 shows the *I-V* behavior of sensor type A1 to the various gases tested with slight differences between them. This suggests minimal charge transfer between the gases and the NTs and, as a result, relatively low sensitivity. As mentioned previously, the overall electrical responses of the sensor using SWCNTs could be due to a number of variables. Namely, the structure of the NTs, e.g., the presence of small diameter NTs, low densities, and the presence of metallic NTs in the percolation network and the sensor configuration, e.g., the distance between the electrodes and metal used. In the case of the sensor A2, the polymer structure should also have been affected by the doping effect from the gas resulting in conductivity changes, as well as polymer doping by counter ions before gas testing "primary doping" . However, similarly to the A1 sensor, the A2 *I-V* behavior in Fig. 2 shows nearly identical responses to the gases as a function of concentration which is also indicative of negligible sensitivity to the gases tested. The polymer did not oxidize as PQT-12 is relatively stable to oxygen, moisture, and light. It is likely that the A2 device senses at higher gas concentration levels. However, we used the same gas concentrations for all the devices to maintain consistency. The most interesting feature from the *I-V* data in Fig. 2 is from sensor A3, the nanocomposite sample. There is no response to N2 as it is an inert gas. There is a higher response to H2, which is reasonable since a small response also occurred

in the A1 sensor. In the case of NH3, changes were observed even at 10 ppb with dramatic *I-V* responses to acetone. From the *I-V* plots in A3, the conductance $G = I/V$ was determined to increase with H2, decrease with NH3, and increase dramatically with acetone. The decrease in conductance when NH3 is present could have resulted from the charge transfer between the two unpaired electrons in N and the nanocomposite or near the nanocomposite/ metal interface. This created an *n*-type material, which decreased the conductance. In the case of acetone, the paired electrons from oxygen may form a *p*-type material with the nanocomposite or nanocomposite/metal interface, resulting

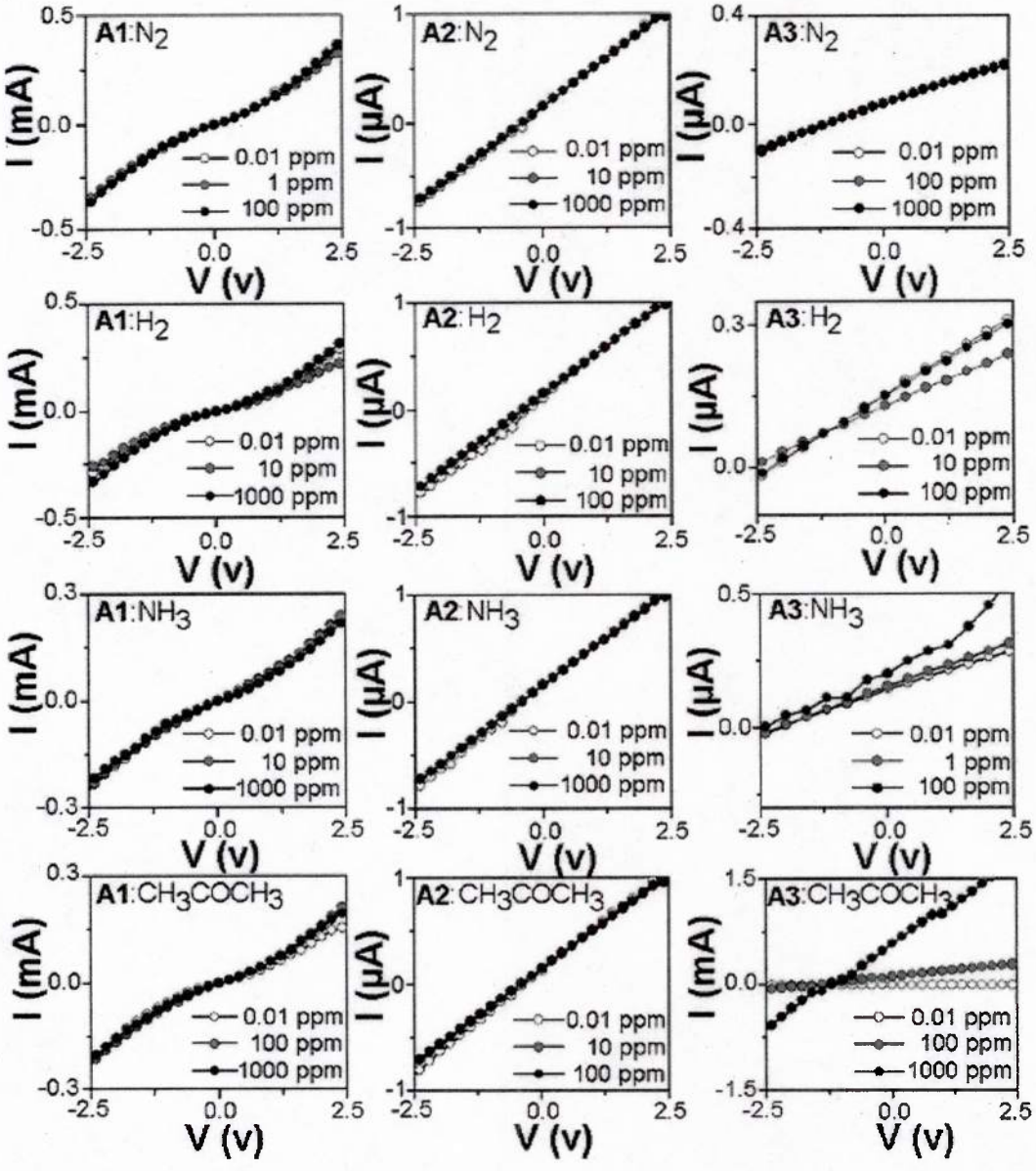

FIG. 2. Measured *I-V* characteristics of the devices A1, A2, and A3 collected from the IDEs located at the center. The gases tested were N_2, H_2, NH_3, and acetone with concentrations varying from 0.01 up to 1000 ppm.

in a dramatic increase in conductance. Previous work has indicated a superior response of CPs to up to thirty-four volatile organic compounds VOCs including alcohols, esters, aromatics, and alkanes, whereas using semiconducting SWCNTs the detection of VOCs is somewhat reduced. By combining the two, the sensitivity of the SWCNTs to VOCs is improved. Figure 3 shows the sensitivity given by $G-G0\ /G0$, where $G0$ is the conductance of the inert gas N2 of the three devices per concentration of gases tested _up to 10 ppm. The graph shows an improved sensitivity of the three gases when using the nanocomposite at 10 ppb, whereas the sensitivity of the A2 sensor is practically zero and the sensitivity of the type A1 sensor is enhanced when the polymer is added. Higher concentrations resulted in slightly better sensitivities, which can be improved by increasing the evacuation time to the subsequent gas. Nevertheless, Fig. 3 clearly indicates an enhanced sensitivity at the lower gas concentration tested. While ultrasonication is commonly used to form the CNT/CP nanocomposites, we simplified the procedure by dropping PQT-12 on top of the NTs. This resulted in a dramatic sensitivity/selectivity compared to the components, thus facilitating sensor scalability. Since the overall effect of the A3 sensor is much larger than in the A1 only NTs or A2 pure PQT-12 sensors, some effects of the modification of charge transfer between the NTs and CPs in the nanocomposite are clearly present. Even using only 1 wt. % NTs, the response at 10 ppb sensitivity even for a vacuum measurement seems to have been multiplied. Therefore, from the *I-V* behavior the nanocomposite material provides the gas sensing mechanism instead of the individual components. The charge transfer between the NT and polymer dopes the polymer and changes the overall conductivity of the system. The amount of transfer depends on where the HOMO of the NT is relative to the LUMO of the polymer (see Fig. 4). The transfer of charge between the HOMO-NT and the LUMOpolymer is a tunneling process and therefore, depends exponentially on the tunneling barrier, i.e., the energy difference between the levels. Consequently, the deeper the HOMO-NT is in the bandgap of the polymer, the lower the charge transfer and the lower the conductivity. If there is a shift in the NT levels relative to the polymer bandgap, even if it is a very small shift, the change in the conductivity of the system will be dramatic due to the exponential change in charge transfer. When a linear property, such as gas exposure, is coupled to an exponential property, such as current flow, then the overall effect is a multiplication of the signal, i.e., "gain" in the chemical sensor. The *I-V* behavior from all the IDE locations tested labeled in Fig. 1_b_ as C, center; RB, right big; LB, left big; DB, down big_ in the three devices resulted in a similar data indicative of IDEs homogeneity within the four membranes. By adjusting the four-membrane sensor, we envision the possibility of using four different nanocomposite materials each sensitive to a particular gas, resulting in selectivity toward gas mixtures. More tests to improve sensitivity/selectivity of the sensors are in preparation.

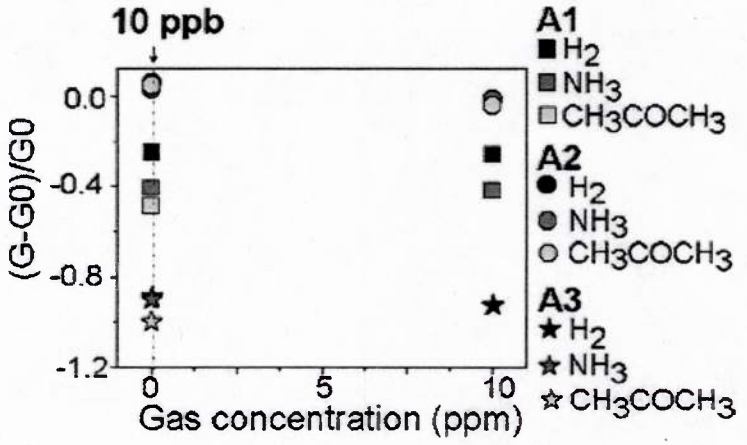

FIG. 3. Sensitivity $[(G-G_0)/G_0)]$ of the three sensors vs the concentrations of the three gases tested. The differences in sensitivity from the three devices are clearly seen at 10 ppb.

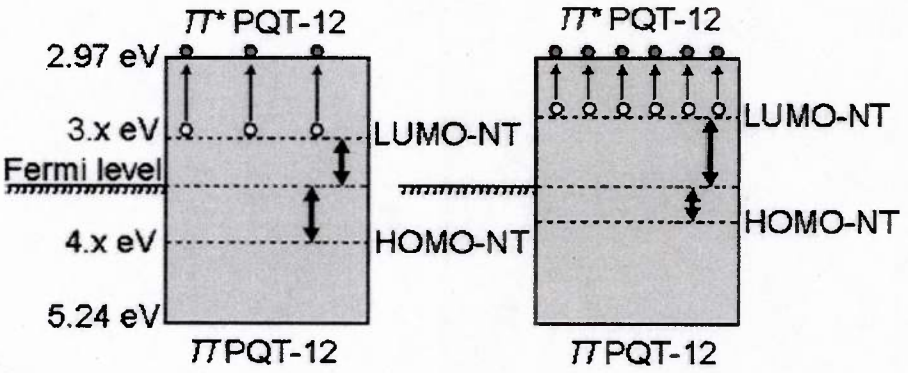

FIG. 4. Schematic representation of the band diagram for the SWCNTs/ PQT-12 nanocomposite.

Plasmonic Pressure Sensors

Plasmonic coupling between closely spaced nanoparticles has been well documented. Small changes in the spacing of closely packed nanoparticles cause a shift in the luorin resonance which can be observed as a redshift or blueshift in the absorption or reflection spectra respectively, of the nanoparticles relative to the spectra of isolated particles. This shift depends on a number of factors including spacing distance, particle shape and size particle morphology orientation the host medium and polarization. This widely known effect is due primarily to the coupling of the near-fields of the surface plasmons together. Since these excitations are charged, a given particle can be seen as sitting within the field of another somewhere in the dispersion. When they are brought closer together the field effects are greater. This is essentially equivalent to saying that the average dielectric constant in a volume increases as the volume becomes more filled with nanoparticles. Details on the various models of this effect can be found in the literature.

This strong relationship between a number of variables and the optical properties of nanoparticle arrays has led to significant interest in using the surface luorin resonance of metal nanoparticles in sensing technology. Use of this phenomenon has been made in length sensing of biological molecules. Binding of gold nanoparticles coated with streptavidin to single-strand and double-strand DNA has shown that the spectral shift in luorin absorption band can be used to determine which type of DNA is present. The length and stiffness of the bound DNA yields a separation between particles that can then be found by determining the luorin resonance peak and using this in an empirically determined luorin ruler equation.

Linking of nanoparticles using proteins has led to humidity sensors based on plasmonic coupling. Gold nanoparticles are assembled into a thin film by using the protein myoglobin as a linking agent. This protein's small size (2.5 nm x 3.5 nm x 4.5 nm) is on the scale of plasmonic coupling, and small changes in humidity can cause relatively large changes in the molecular shape. This in turn causes changes in the interparticle spacing which can be detected as a shift in the luorin resonance. The device can sense changes in the relative humidity as small as 1% with rapid recovery.

Metal nanoparticles arrays have also shown usefulness as sensors of refractive index. Nanoparticle arrays self-assembled on a Poly(4-vinylpyridine) modified glass substrate, then placed in solvents of various refractive indices, have shown significant shifts in the luorin absorption spectrum. Gold nanoparticles have also shown strong shifts in spectra when placed in solvents of differing refractive indices This effect is due to the strong dependence of the localized surface luorin resonance (LSPR) on the dielectric constant of the host medium in contact with the nanoparticle's surface as mentioned above.

Nanoparticle arrays assembled in polymer matrices have also shown interesting optical properties. Random arrays in Polydimethylsiloxane (PDMS) have shown significant spectral shifts due to stretching of the polymer medium which results in an increase in the spacing of the nanoparticles. Stretching of the PDMS thin film by 50% showed a shift in

the absorption spectrum from a strong peak at 436 nm, indicative of coherent interactions between the embedded to nanoparticles, to a spectrum with peaks at 430 nm and 545 nm, indicative of non-interacting nanoparticles of the dimensions used. These results argue that polymer/nanoparticle composite systems can be used to sense mechanical changes in the polymer matrix.

Our pressure sensor uses the plasmonic coupling between particles to sense pressure. Nanoparticles closely spaced in a dielectric medium will exhibit plasmonic coupling and thus experience a shift in their resonance. If these nanoparticles are placed in a compressible material then exposure to pressure will reduce the interparticle distance and give rise to a shift in the luorin resonance band. The pressure sensitivity of this polymer/nanoparticle composite is strongly dependent on the mechanical properties of the matrix. Low bulk modulus materials, such as PDMS, compress more easily under pressure, providing a larger change in interparticle spacing and thus a larger shift in the luorin resonance for a given applied pressure. The governing equation relating bulk modulus B to the applied pressure is:

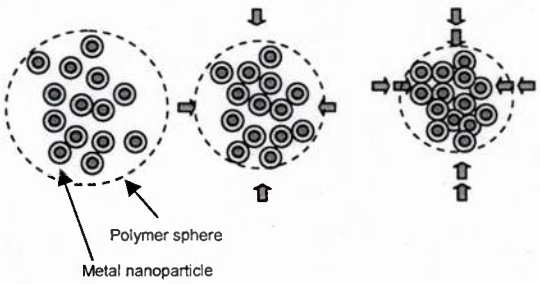

$$B = \Delta P \cdot \frac{S_0}{\Delta S} \qquad \text{(Eq. 1)}$$

Model for microsphere pressure sensor

where ΔP is the change in applied pressure, S_0 is the relaxed interparticle spacing, and ΔS is the change in volume. Literature suggests that for 30nm silver nanospheres with an interparticle spacing of 30nm every 1nm of shift in the luorin resonance corresponds to a change in interparticle spacing of 0.3nm. Assuming we wish to see a 5nm shift for confident pressure measurement we would need an applied pressure of 80 mm Hg. In the bulk material this assumes that all interparticle interactions are operating over this length scale of 30nm; in fact even in a perfectly ordered system many interactions will take place over a variety of length scales. In a random arrangement of particles we have a continuum of spacings and so a continuum of interaction potentials and associated luorin resonance shifts. This would contribute to an averaging effect which would wash out any detectable shift.

Chumanov et.al. have shown that in randomly disbursed nanocomposite materials significant changes can be seen in the absorption spectrum with changes in interparticle spacing of a much larger magnitude than that of the model above. Stretching a thin film of PDMS with embedded silver nanoparticles resulted in two effects: a decrease in absorption as the optical path encounters less film and coherent interactions between particles played less of a role, and a shift in the in the resonance peak as the interparticle

spacing increased enough to overcome the averaging effects. The film in this work was stretched by 50%, showing that significant stretching must occur in order for this effect to be seen. Plugging in a compression of 50% in equation 1 shows that we would need a host matrix with a maximum bulk modulus of about 25 kPa.

This bulk modulus lies an order of magnitude below that of the most compressible bulk polymers. However a number of material designs allow us to obtain bulk moduli on this order. Foams are widely available with bulk moduli of less than 50 kPa, putting us in the realm where the pressure sensor becomes feasible. Incorporation of nanoparticles into the filaments of the foam is easily achieved. While the material in the foam still compresses minimally along the filament axis, with sufficiently small pore size the particles could interact across the pores. As the material compressed this distance would decrease, giving rise to the desired change in absorption spectrum. The development of nanofoams provides a material with pore sizes on the order of particle-particle interactions, a promising avenue for further research.

Also of interest have been aerogels. These materials include large volumes of air throughout the matrix and are highly compressible. While initial separations between particles would be large, relatively small pressures could collapse the aerogel enough to cause interactions to become a part of the optical picture yielding a significant change in luorin resonance. Since the filaments of polymer in these materials are very small they would experience large deformations under stress, yielding a secondary luorin resonance shift.

Foams and aerogels provide a second possible mechanism for luorin resonance shifts. As these materials compress and the volume ratios of foam material to air change the average dielectric of the material will also change. It is easy to show that the frequency/wavelength of the luorin resonance is related to the dielectric of the host medium through the equation:[i]

$$\lambda_{sp} \propto \sqrt{\frac{\varepsilon_1 \varepsilon_2}{\varepsilon_1 + \varepsilon_2}} \qquad \text{(Eq. 2)}$$

where λ_{sp} is the peak wavelength of the surface luorin and $\varepsilon_1, \varepsilon_2$ are the real part of the dielectric function of the metal nanoparticle and the host medium. As the average dielectric of the foam changes we would expect to see a change in this resonance wavelength. Assuming a foam dielectric constant of 2.5, the average dielectric of a foam with 50% volume filled by air would be 1.75. Compression of the foam by 20% yields only 30% air in the volume, and a corresponding shift in the average dielectric to 2.05. This change would, by the equation above, yield a shift in the luorin resonance of 5.5 nm.

Our preliminary results are shown here in figure 1.

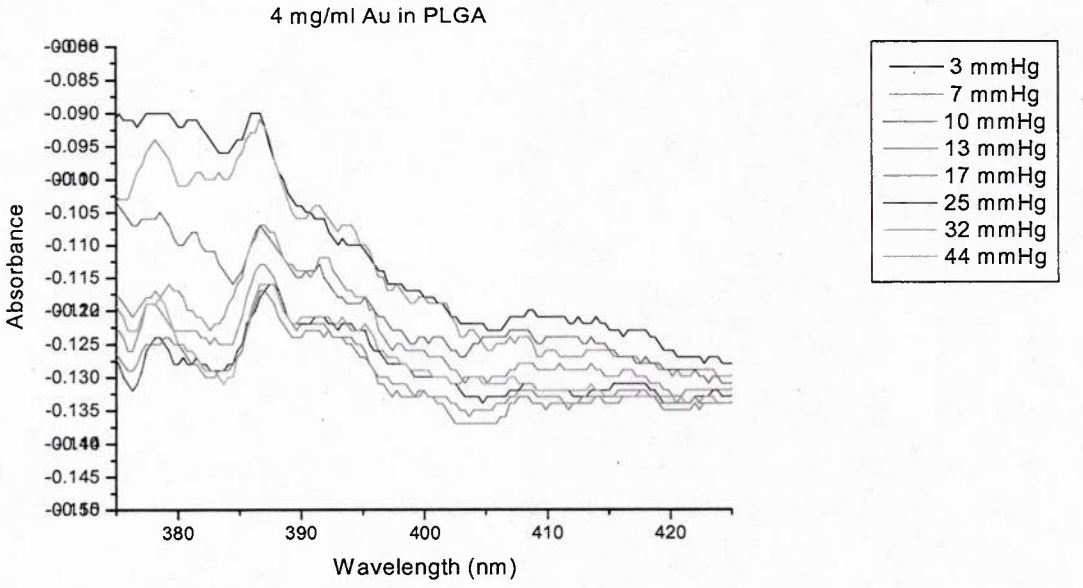

From the raw data above we calculate pressure below in figure 2

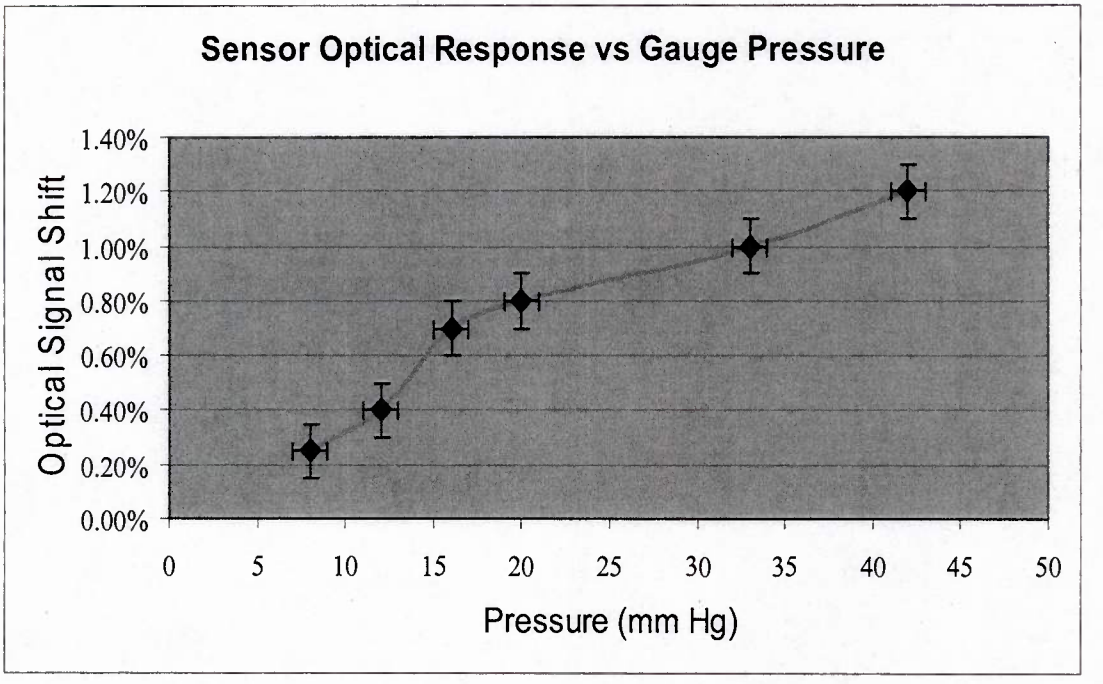

This report lists only the major advances of the program and is NOT exhaustive.

Novel New electroluminescent polymers

1. Synthesis of 4,7-dibromo-2,1,3- benzothiadiazole

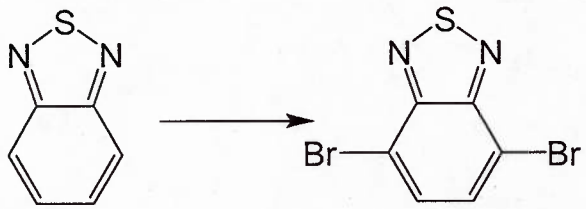

A mixture of 136 g (1.0 mole) of 2,1,3- benzothiadiazoles in 200 ml of 47% HBr was heated under reflux with stirring, while 480 g (3.0 moles, 165 ml) of bromine was added slowly within 3.20 hours. [Towards the half-way point of the addition, GLC indicated the following composition of the reaction mixture: 30% of 2,1,3-benzothiadiazoles, 60% of 4-bromo-2,1,3-benzothiadiazole, and 10% of 4,7-dibromo-2,1,3- benzothiadiazole.] Towards the end of the addition, the reaction mixture became a suspension of solid in the hydrobromic acid. In order to facilitate stirring, 100 ml of 47% HBr was added and the mixture was heated under reflux for 2.5 hours after completion of the bromine addition. The mixture was filtered while hot, cooled, filtered again, washed with water and dried to give 305 g (95%) of 4,7-dibromo-2,1,3- benzothiadiazole. [mp = 188-189°C]

2. Synthesis of 2,7-dibromo-9,9-didecylfluorene

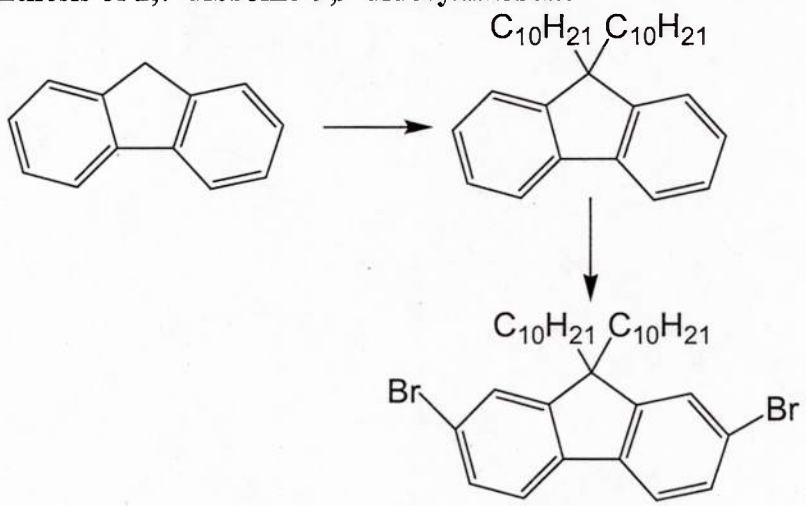

An aliquot of 214.6 mmol of n-butyllithium was added dropwise to a solution of luorine in THF (210 ml) at -78 °C. The mixture was stirred at-78 °C for 1 h, and (235.06 mmol) decyl bromide in THF (40 ml) was added dropwise to the mixture, which was stirred for 30 min. The solution was allowed to warm to room temperature and was stirred for 4 h. The mixture was poured into water and extracted with diethyl ether. The organic extracts were washed with brine and dried over $MgSO_4$. The solvent was removed by rotary evaporation. Excess decyl bromide was removed by distillation (100 °C oil bath, 0.3 Torr or 300 mbar) to give 9,9-didecyl luorine.

This report lists only the major advances of the program and is NOT exhaustive.

Under nitrogen, 0.1 mol of 9,9-didecylfluorene was placed in a 500 ml round-bottomed flask. After the addition of 300 ml of dry DMF, (0.3 mol) bromine was added slowly. The mixture was allowed to react for 20 h at room temperature, and then saturated $NaHSO_3$ was added until the red color disappeared. The mixture was extracted three times with 200 ml of diethyl ether. The organic extracts were combined, washed with brine, and dried with $MgSO_4$. Upon filtering the solution and evaporating the solvent, the crude 2,7-dibromo-9,9-di-n-decylfluorene was obtained, which was recrystallized in hexane at 0 °C to give pure product.

3. Synthesis of 2,7-Bis(4,4,5,5-tetramethyl-1,3,2-dioxaborolan-2-yl)-9,9 didecylfluorene

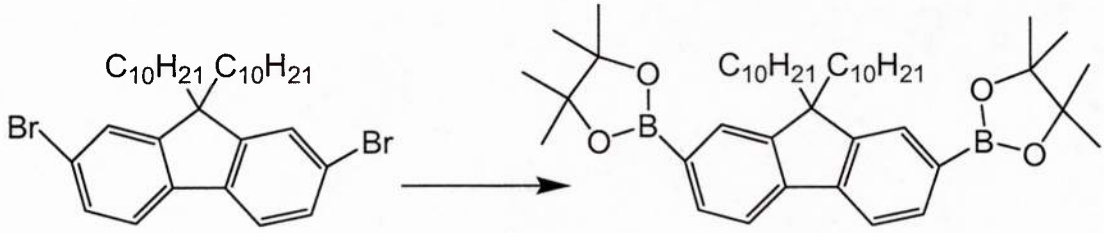

To a solution of 2,7-dibromo-9,9-didecylfluorene (12.8 mmol) in THF (120 ml) at -78 °C was added, by syringe, (57.42 mmol) of n-butyllithium (1.7 M in hexane). The mixture was stirred at -78 °C for 2 h. 2-Isopropoxy-4,4,5,5-tetramethyl-1,3,2-dioxaborolane (38.4 mmol) was added to the solution, and the resulting mixture was stirred at -78 °C for 1 h, warmed to room temperature, and stirred for 40 h. The mixture was poured into water, extracted with dichloromethane, and dried over $MgSO_4$. The solvent was removed by solvent evaporation, and the residue was purified by several reprecipitations in hexane to provide the product.

4. Preparation of Tetrakis(triphenylphosphine) palladium (0) $(PPh_3)_4Pd(0)$

To a solution of palladium dichloride (0.25 g, 1.41 mmol) in dimethyl sulfoxide (DMSO, 17 ml) was added 1.85 g (7.06 mmol) of triphenylphosphine. The system was kept under an argon atmosphere. The mixture was heated at 140 °C until complete solubilization occurred. The heated bath was then taken away, and the solution was rapidly stirred for approximately 15 min. Hydrazine hydrate (0.28 ml) was added over 1 min. A vigorous reaction took place with a water bath; crystallization began to occur at 125 °C. At this point the mixture is allowed to cool without the use of the water bath. After the mixture reached room temperature, it was filtered under argon on a coarse, sintered-glass funnel. The solid was washed successively with two 15 ml portions of ethanol and two 15 portions of diethyl ether. The product was stored under an inert atmosphere.

5. Synthesis of 1,4-dibromo-2,5-dimethylbenzene

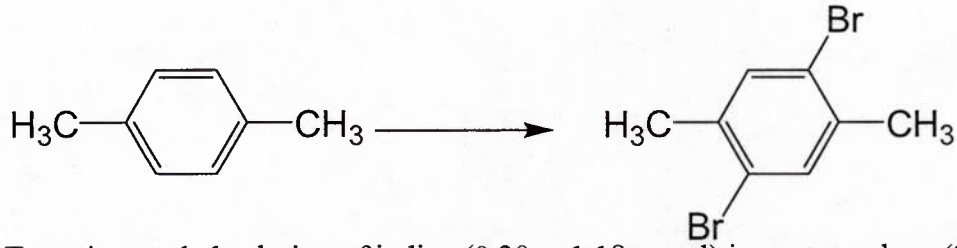

To an ice-cooled solution of iodine (0.30 g, 1.18 mmol) in neat p-xylene (23.1 ml, 0.19 mol) was added bromine (19.8 ml, 0.385 mol) dropwise over 1 h in the absence of light. After 16 h at room temperature 20% aqueous KOH (100 ml) was added. The mixture was shaken under slight warming until the disappearance of the yellow color and was then allowed to cool. The aqueous layer was decanted, and the remaining solids were washed with water (4×50 ml). Recrystallization from absolute ethanol gave 1,4-dibromo-2,5-dimethylbenzene as white crystals. [mp = 72-74 °C]

6. Synthesis of 1,4-dibromo-2,5-bis(bromomethyl) benzene

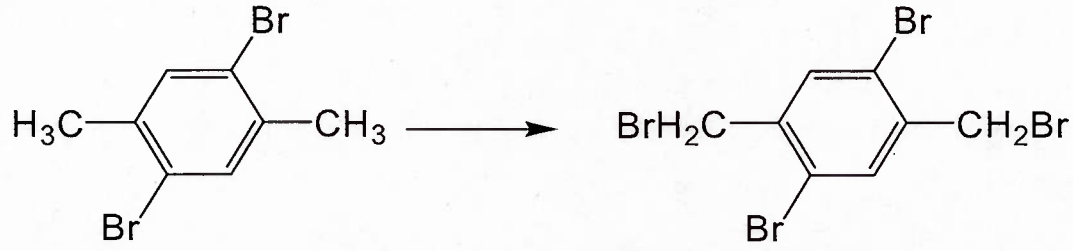

A mixture of 1,4-dibromo-2,5-dimethylbenzene (20.4 g, 77.1 mmol), N-bromosuccinimide (28.3 g, 0.159 mol), and 1,1'-azobis(cyclohexanecarbonitrile) (0.010 g, 0.041 mmol) in benzene (380 ml) was heated at reflux for 8 h. The solvent was removed in vacuum and recrystallization with absolute ethanol afforded 1,4-dibromo-2,5-bis(bromomethyl)benzene as white crystals. [mp = 156-158 °C]

Method II

2,5-dibromo-*p*-xylene (10g, 38 mmol) was treated with *N*-bromosuccinimide (16g, 91 mmol) in carbon tetrachloride (100 ml). A small amount of benzoyl peroxide was add as initiator. The reaction mixture was refluxed at 80°C for 5 h under N_2 gas. The completion of the reaction was indicated by the appearance of succinimide on the surface of the reaction solution. The solution was concentrated and precipitated from methanol.

7. Synthesis of 1,4-dibromo-2,5-bis(bromomethyl)benzene triphenyl phosphonium salt

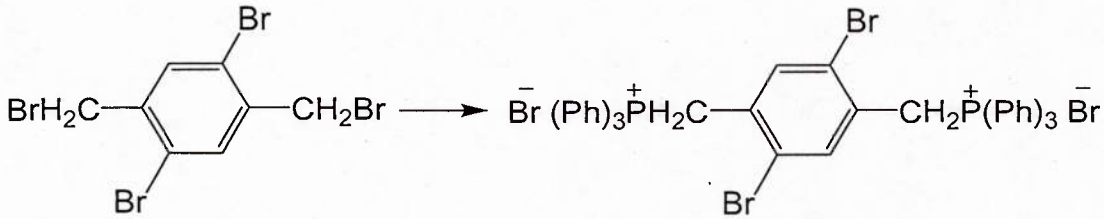

A mixture of 1,4-dibromo-2,5-bis(bromomethyl)benzene (12.4 mmol), triphenyl phosphine (37.2 mmol) and 30 ml of DMF was heated to reflux for 2 h. The reaction mixture was cooled to room temperature. The product was filtered, washed with ether, dried in vacuum and recrystallizied from ethanol to give pure monomer.

Method II

A solution of 1,4-dibromo-2,5-bis(bromomethyl)benzene (12g, 28 mmol) and triphenyl phosphine (22g, 85 mmol) in dimethyformamide (100 ml) was stirred and heated to reflux for 24 h. The resulting mixture was poured into diethyl ether. After filtration and vacuum drying, 1,4-dibromo-2,5-bis(bromomethyl)benzene triphenyl phosphonium salt was obtained as a white powder

8. Synthesis of 1,4-dibromo-2,5-bis(4-pyridinyl)benzene, 1,4-dibromo-2,5-bis(2-thiophenyl)benzene, 1,4-dibromo-2,5-bis(8-quinolinyl)benzene

1 mmol of 1,4-dibromo-2,5-bis(bromomethyl)benzene triphenyl phosphonium salt **[I]** and 2 mmol of 4-pyridinecarboxaldehyde [**II**] were dissolved in a mixture of 60 ml of anhydrous ethyl alcohol and 20 ml of chloroform in a three-neck flask, and 2.3 g of 5% solution of sodium metal in anhydrous ethyl alcohol was added dropwise through syringe. The mixture was kept at room temperature for 12 h and 1 ml of 0.1 N aqueous HCl solutions was added to it to end the reaction. The product **[V]** was washed thoroughly with water and methyl alcohol, and then dried in a vacuum oven set temperature at 40 °C.

In the case of 2-thiophenecarboxaldehyde **[III]** and 8-quinolinecarboxaldehyde **[IV],** the reaction was same as 4-pyridinecarboxaldehyde [**II**].

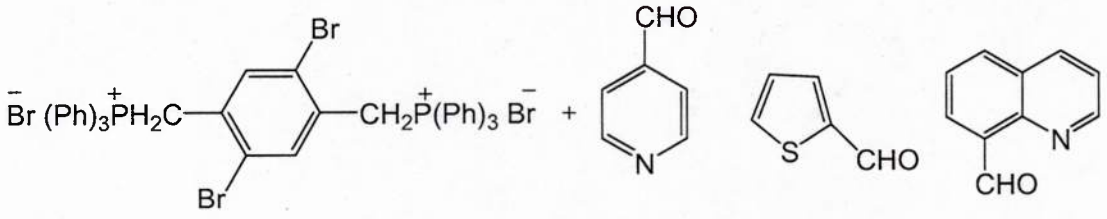

[I] [III] [IIII] [IV]

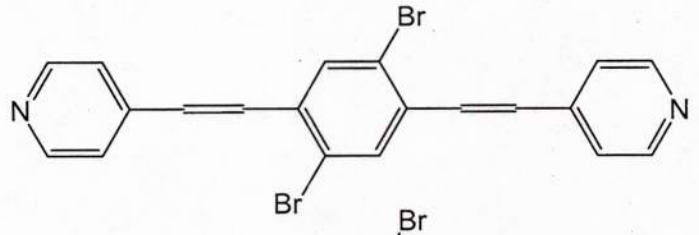

[V]

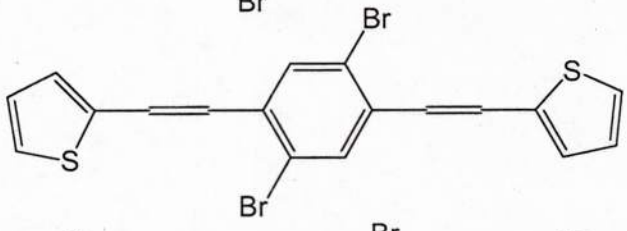

[VI]

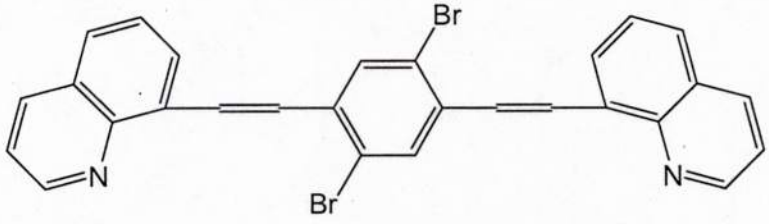

[VII]

9. Polymerization

To a stirred mixture of 4,7-dibromo-2,1,3- benzothiadiazole, 2,7-Bis(4,4,5,5-tetramethyl-1,3,2-dioxaborolan-2-yl)-9,9-didecylfluorene, 7-dibromo-9,9-didecylfluorene, [V], [VI], [VII], $Pd(Ph_3)_4$, and toluene under argon was added tetraethylammonium hydroxide. The reaction mixture was kept stirring for 24 h at 100 °C. After cooling, the resulting mixture was filtered, and the polymer was precipitated by dropwise addition to methanol. The precipitated polymer was collected, washed with methanol, dried under high vacuum of copolymer.

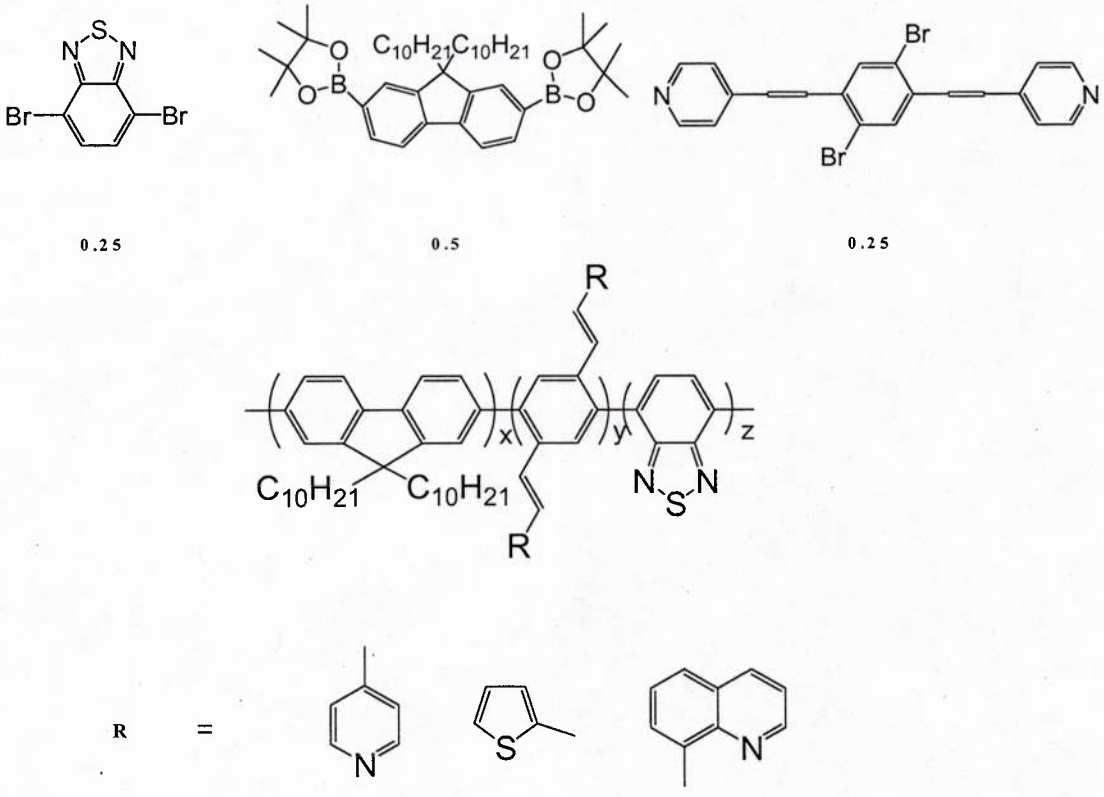

Analysis of this product is underway and will be reported in the next report.

STATS

Personnel Supported:

Ms. Faith Coldren	½ student	microscopy
Dr. Reyes-Reyes	½ time postdoc	Device building
Mr. Scott Webster	student	optical metrology
Dr. David L. Carroll	PI	
Dr. Kyung Kon Kim	Postdoc Associate	photonic crystals
Dr. Jiwen Liu	Postdoc Associate	Devices
Dr. Manoj Namboothiry	Postdoc Associate	Devices

This report lists only the major advances of the program and is NOT exhaustive.

Papers:

1. Scott Webster, Marisol Reyes-Reyes, Xavier Pedron, Román López-Sandoval, Mauricio Terrones, and David L. Carroll, "Enhanced Nonlinear Transmittance by Cooperative Nonlinear Mechanisms: a reverse saturable absorbing carbocyanine dye blended with nonlinear scattering carbon nanotubes" Advanced Materials Volume 17, Issue 10, May, 2005, Pages: 1239-1243 (2005)
2. Kyungkon Kim, Scott Webster, Nicole Levi, Mauricio R. Pinto, Kirk S. Schanze, and David. L. Carroll, Luminescent Poly(phenylene ethynylene) Coated Silica Opals, 21(11) Langmuir, pp 5207 – 5211 (2005)
3. Hua Bao, George Chumanov, Richard Czerw, David L. Carroll, Stephen H. Foulger; Colloid Polym Sci (2005) 283: 653–661.
4. Woo HS, Kim YB, Czerw R, Carroll DL, Ballato J, Ajayan PM; Tailoring hole transport in organic light-emitting devices using carbon nanotube-polymer nanocomposites Journal of The Korean Physical Society (2004) 45 (2): 507-511.
5. Kyungkon Kim and David L. Carroll, Roles of Au and Ag Nanoparticles in Efficiency Enhancement of Poly(3-octylthiophene) / C60 Bulk Heterojunction Photovoltaic Devices, Applied Physics Letters, 87, 203113 (2005).
6. Marisol Reyes-Reyes, Kyungkon Kim, David L. Carroll, High Efficiency Photovoltaic Devices based on Annealed Poly(3-hexylthiophene) and 1-(3-methoxycarbonyl)-propyl-1-phenyl-(6,6)C61 Blends, Appl. Phys. Lett. 87, 083506 (2005)
7. Curran, SA; Talla, JA; Zhang, D; Carroll, DL, Defect-induced vibrational response of multi-walled carbon nanotubes using resonance Raman spectroscopy, *JOURNAL OF MATERIALS RESEARCH*, 20 (12): 3368-3373 DEC 2005
8. J. Liu and D.L. Carroll, Temperature and Flow Rate of NH3 Effects on Nitrogen Content and Doping Environments of Carbon Nanotubes Grown by Injection CVD Method, J. Phys. Chem. B.; (Article); 2005; 109(33); 15769-15774
9. B. Berzina, L. Trinkler , R. Krutohvostov, R. T. Williams , D. L. Carroll, R. Czerw, E. Shishonok , Photoluminescence excitation spectroscopy in boron nitride nanotubes compared to microcrystalline h-BN and c-BN, physica status solidi I Volume 2, Issue 1 , Pages 318 – 321 (2005)
10. Reyes-Reyes, M.; Kim, K.; Dewald, J.; Lopez-Sandoval, R.; Avadhanula, A.; Curran, S.; Carroll, D.L., Meso-Structure Formation for Enhanced Organic Photovoltaic Cells, Org. Lett.; 2005; 7(26); 5749-5752.
11. Liu, J; Czerw, R; Carroll, DL, Large-scale synthesis of highly aligned nitrogen doped carbon nanotubes by injection chemical vapor deposition methods *JOURNAL OF MATERIALS RESEARCH*, 20 (2): 538-543 FEB 2005
12. Woo, HS; Cho, S; Kwon, TW; Park, DK; Kim, YB; Czerw, R; Carroll, DL; Park, JW, Truly blue organic light-emitting diodes based on carbazole-doped 4,4 '-Bis[carbazolyl-(9)]-stilbene, *JOURNAL OF THE KOREAN PHYSICAL SOCIETY*, 46 (4): 981-984 APR 2005
13. Kyong Kon Kim, Jiwen Liu, and D.L. Carroll, Thermal Diffusion Processes in Bulk Heterojunction Formation for Poly-3-hexylthiophene / C60 Single Heterojunction Photovoltaics, Appl. Phys. Lett. 88, 181911 (2006)
14. D.L. Carroll, Polymer solar cells achieve 5.2% efficiency, LASER FOCUS WORLD, 42 (2): 11-11 FEB 2006.
15. J. Liu, S. Webster and D.L. Carroll, Highly Aligned Helical Nitrogen Doped Carbon Nanotubes Synthesized by Injection Assisted Chemical Vapor Deposition, Appl. Phys. Lett. 88, 213119 (2006).
16. A. G Manoj, T. Zimmerman, F. M. Coldren, J. Liu, K. Kim, D. L. Carroll, "Electrochromic Properties of Conducting Polymer Metal Nanoparticles Composites" Submitted to Synthetic Metals (2006).
17. D. L. Carroll, R. Czerw, and B. S. Harrison, "Carbon Nanotube – Poly 3-octylthiophene Composite Photovoltaic Cells" J. Nanosci. Nanotechnol. 6, 2204–2207 (2006)
18. B. Berzina, L. Trinkler, V. Korsak, R. Krutohvostov, D. L. Carroll, K. B. Ucer and R. T. Williams, Exciton luminescence of boron nitride nanotubes and nano-arches Physica Status Solidi (b) Vol. 243/14/2006, page 3840-3845

This report lists only the major advances of the program and is NOT exhaustive.

19. F.-X. Zha, S. Roth and D.L. Carroll, Periodic, pearl chain-like nanostructure observed by scanning tunneling microscopy, Carbon, Volume 44, Issue 9, August Pages 1695-1698 (2006)
20. Vieira SMC, Stephan O, Carroll DL, Effect of growth conditions on B-doped carbon nanotubes, JOURNAL OF MATERIALS RESEARCH 21 (12): 3058-3064 DEC 2006
21. Curran S, Dewald J, Carroll DL, All-optical nanoscale read/write bit formation, JOURNAL OF MICROLITHOGRAPHY MICROFABRICATION AND MICROSYSTEMS 5 (1): Art. No. 011013 JAN-MAR 2006
22. Liu J, Carroll DL, Cech J, Roth S, Single-walled carbon nanotubes synthesized by the pyrolysis of pyridine over catalysts, JOURNAL OF MATERIALS RESEARCH 21 (11): 2835-2840 NOV 2006
23. Curran SA, Zhang DH, Wondmagegn WT, Ellis AV, Cech J, Roth S, Carroll DL, Dynamic electrical properties of polymer-carbon nanotube composites: Enhancement through covalent bonding, JOURNAL OF MATERIALS RESEARCH 21 (4): 1071-1077 APR 2006
24. Jiwen Liu, Manoj A. G. Namboothiry, and David L. Carroll, Fiber-based architectures for organic photovoltaics Appl. Phys. Lett. 90, 063501 (2007
25. Jiwen Liu, Manoj A. G. Namboothiry, and David L. Carroll, Optical geometries for fiber-based organic photovoltaics Appl. Phys. Lett. 90, 133515 (2007) (reprinted in the Virtual Journal of NanoSciences)
26. Kyong Kon Kim, Jiwen Liu, Manoj Namboothiry, David L. Carroll, The roles of donor and acceptor nanodomains in 6% efficient thermally annealed photovoltaic devices, Appl. Phys. Lett. 90, 163511 (2007).
27. R. T. Williams, K. B. Ucer, D. L. Carroll, B. Berzina, L. Trinkler, V. Korsak, R. Krutohvostov, Photoluminescence of self-trapped excitons in boron nitride nanotubes, accepted to JNN (2006)
28. Scott Webster*, Richard Williams, David L. Carroll, Enhanced Absorption in a Reverse Saturable Dye Blended with Carbon Nanotubes, accepted to JNN (2006)
29. R Jayakanth, A G Manoj, J Liu, I Manna and D L Carroll, "A Novel Polymer Nanotube Composite for Photovoltaic Packaging Applications" submitted to Synthetic Metals (2007)
30. J.E. Kielbasa, J. Liu, K.B. Ucer, D.L. Carroll, and R.T. Williams, "Sol-gel nanocomposites as metamaterials: preparation and optical measurements" accepted Journal of Materials Science: Materials in Electronics
31. M. Reyes-Reyes, R. López-Sandoval, J. Liu, and D.L. Carroll "Bulk heterojunction organic photovoltaic based on polythiophene-polyelectrolyte carbon nanotube composites", in press Thin Solid Films (2007)

Invited lectures at international meetings:

1. International Workshop on Conjugated Polymers "Carbon Nanotube Cancer Therapeutics" Wollongong Australia (Feb 2007)

2. International Workshop on Conjugated Polymers "High efficiency photovoltaics" Wollongong Australia (Feb. 2007)

3. International Conference on Defects in Materials (ICDIM) "Negative Index Materials" Prague Czech Republic (June 2006)

4. International Conference on Synthetic Metals "High efficiency Solar Cells" Dublin Ireland (June 2006)

5. International Winter School "High Efficiency Solar Cells" Kirchberg Austria (March 2006)

6. Optical Society of America "High Efficiency Solar Cells" Uncasville (CT) (April 2006)

7. American Chemical Society (Colloid Section) "Colloidal Crystals with Conjugated Systems" Potsdam, NY (June 2005)

This report lists only the major advances of the program and is NOT exhaustive.

8. Int. Conf. on Quantum Transport and Quantum Functional Materials "Advances in Organic Device Technologies" Bologna, Italy (June 2005)

9. American Chemical Society "Applications of Iron Filled Nanotubes" San Diego, CA (April 2005)

10. International Conference on Synthetic Metals "Advances in nanocomposite based devices" Wollongong, Australia (June 2004)

11. American Physical society Regional Meeting "Advances in Organic Device Physics" Oak Ridge TN (Nov 2004)

12. Optical Society of America, Optics in the Southeast "Optical limiting in carbon nanotubes and their variants" Charlotte, NC (Nov. 2004)

13. Nanotec' 04 "Advances in nanocomposite-based devices" Batz-Sur-Mer, France (Aug 2004)

14. ISOPL (International Society for Optical Power Limiting) "Optical Limiting in Carbon Nanotubes: Materials Modifications" Tucson, Az. (April 2004)

Patents:

D. Carroll, Manoj Namboothiry, Jiwen Liu, "Organic optoelectronic devices and applications thereof" (PCT filed May 1, 2006)

D. Carroll, Nicole Levi, Faith Coldren, "Methods and compositions for printing biologically compatible nanotube composites" (Provisional filed April 2006)

D. Carroll, S. Curran, "Fiber photovoltaic devices and applications thereof" (Provisional filed May 1, 2006)

D.L. Carroll, S. Akman, F. Torti, S. Torti, O. Nakasuma, P.M. Ajayan, "Novel carbon nanostructures for cancer therapeutics" (Provisional filed May 2006)

D. Carroll, Nicole Levi, Faith Coldren, Manoj Namboothiry, Larry Webb, Thomas Smith, William Wagner, "Novel Nano-Scale pressure sensors" (provisional filed Jan. 2006)

D. Carroll, Nicole Levi, John Stewart, "Novel Oxilaplatin delivery mechanisms for Cancer therapeutics" (Disclosure filed May 2006)

D. Carroll, Manoj Namboothiry, Jiwen Liu, "Nanocomposite lighting system" (provisional filed 2006)

D Carroll, Manoj Namboothiry, Jiwen Liu, "Thermal treatment of thin film photovoltaics" (provisional filed 2006)

(all list AFOSR funding)

This report lists only the major advances of the program and is NOT exhaustive.

Transitions:

Carroll, Wake Forest University, b. nanoparticles for Surfaced Enhanced Raman, c. Transition to David Rauh, EIC Corp Waltham MA, d. Testing for possible insertion in hand-held bio-sensor.

Carroll, Wake Forest University, b. nanocomposites for OLEDs c. Transition to Yazaki Meter Corporation Susono City Japan, d. Testing for possible insertion into dashboard displays. (This transition possibility consists of assignment of IP rights).

Carroll, Wake Forest University, b. nanocomposites for solid state lighting c. Transition to Daryl Beaudreux Nanoholdings Inc NJ, d. licensing for company startup.

Carroll, Wake Forest University, b. fibercell technologies for advanced organic photovoltaics c. Transition to Daryl Beaudreux Nanoholdings Inc NJ, d. licensing for company startup.

Carroll, Wake Forest University, b. ordered nanocomposites for photovoltaics c. Transition to Konarka Inc Lowell MA, d. testing for possible licensing opportunities.

Carroll, Wake Forest University, b. ordered nanocomposites for photovoltaics c. Transition to Plextronics Inc Pittsburg PA, d. testing for possible licensing opportunities.

Honors

Dr. Carroll named Fellow of the Society for Nanoscience and Nanotechnology

END

This report lists only the major advances of the program and is NOT exhaustive.